VIP Tumor Cells

DOI: 10.1002/ange.201108695

Sensitive and High-Throughput Isolation of Rare Cells from Peripheral Blood with Ensemble-Decision Aliquot Ranking**

*Perry G. Schiro, Mengxia Zhao, Jason S. Kuo, Karen M. Koehler, Daniel E. Sabath, and Daniel T. Chiu**

The challenge of isolating rare cells is often a stumbling block for research in circulating tumor cells (CTCs) fetal cells in maternal blood[3] and cancer stem cells. A better understanding of these cells is important for progress in personalized medicine. Of particular interest is single-cell analysis of CTCs as a marker of cancer metastasis and disease progression.[6,8] These rare cells are present at such low levels (average of 1–10 CTCs per milliliter)[9] that traditional methods, such as flow cytometry, are inadequate. To address this challenge, a number of approaches have been explored in recent years, such as immuno-magnetic isolation as exemplified by the commercial CellSearch system,[2,10] cell-size based filtration method,[11,12] antibody-based surface capture in tailored microfluidic devices,[13–16] wide-field optical imaging with fiber-optic array scanning technology (FAST),[17] passive cell sorting,[18] and negative selection approaches.[19] Although these methods represent important advances in this field, much improvement is still needed to isolate CTCs. For example, conditions for immuno-magnetic isolation can be damaging to cells.[2] In other methods, red blood cells (RBCs) are often lysed prior to screening for CTCs in the remaining white blood cells (WBCs), which can cause cell stress. In many approaches, the recovery of CTCs after imaging can also be challenging.[20] Size-based separation methods have certain advantages, but this technique will miss CTCs that are smaller than others.[11,13] Antibody-based surface capture methods have excellent detection of CTCs in cancer patients. The captured CTCs, however, can be difficult to remove from the surface without cleaving cell-surface proteins (e.g. with Trypsin) and thus potentially stressing the cells. Subsequent imaging of the captured CTCs can also be time consuming, owing to the large area over which images must be taken. Here, we describe an approach that is different from what has been so far explored in this area of research and which we believe offers significant advantages.

Our method is based on positive selection, where cell-surface markers are labeled with fluorescent antibodies, ranked by aliquots, and sorted. We call this process ensemble-decision aliquot ranking (eDAR), because we perform the ranking by looking at an ensemble of cells within each aliquot. In our method, we break down a blood sample into nanoliter aliquots that get rapidly ranked for the presence or absence of CTCs; the ranking helps us to decide which aliquots of cells are worth closer investigation. Our current microfluidic platform can routinely analyze 1 mL of the whole blood in 20 min with a recovery efficiency of greater than 93% ($n=9$) and a false positive rate of zero ($n=8$). Most importantly, this platform enriches CTCs into a small field-of-view ($<1\ mm^2$) for microscopic imaging and allows easy isolation of and access to individual live CTCs for further downstream analysis and culture.

The eDAR process is operationally similar to flow cytometry but with important differences. The throughput of traditional flow cytometry is limited by the sequential analysis of individual cells in a single-file format; the process may take over 24 h for 1 mL of blood containing five billion blood cells.[21] To greatly increase throughput, eDAR probes for rare cells in nanoliter aliquots of blood that each contain thousands of cells. Once the aliquots containing CTCs have been collected, blood cells, especially RBCs, are removed from the CTCs by an on-chip filtration system. The eDAR process is extremely efficient at enriching rare cells. If there are five CTCs in 1 mL of blood, eDAR will discard 99.999% of the blood volume and present a combined 10 nL of blood within a small accessible area ($<1\ mm^2$) of the filter. The isolated CTCs can be imaged on the filter or selectively removed for additional single-cell studies.

The first step in eDAR is to generate or define an aliquot. We initially focused on aliquoting blood into droplets;[22,23] Figure 1b shows a continuous stream of aliquots defined by droplets surrounded by an immiscible phase. We had presumed that encapsulation of the cells in a droplet may protect the cells from flow and associated stresses outside of the droplet. This assumption may be too simplistic because recirculation flow present within droplets can generate significant hydrodynamic shear stresses on cells.[24] In addition, we found that droplets have other disadvantages. First, because droplets were spaced apart by immiscible oils, the throughput was reduced by at least half at a given flow rate through the interrogation region. Second, the generation and stability of the droplet stream was highly sensitive to flow conditions, an unwanted characteristic that compromised the operational

[*] P. G. Schiro,[+] M. Zhao,[+] J. S. Kuo, Prof. D. T. Chiu
Department of Chemistry, University of Washington
Box 351700, Seattle, WA, 98195 (USA)
E-mail: chiu@chem.washington.edu
K. M. Koehler, Prof. D. E. Sabath
Department of Laboratory Medicine and Medicine
University of Washington, Seattle, WA, 98195 (USA)

[+] These authors contributed equally to this work.

[**] We wish to thank the patients who enabled this research, as well as Roy Olund for constructing the dedicated electronic sorting processor, Gavin Jeffries for help with blood droplet formation, and Gabriele Shuster for arranging patient samples. This work was supported by the Life Sciences Discovery Fund and the National Institutes of Health (grant number R21CA147831).

Supporting information for this article is available on the WWW under http://dx.doi.org/10.1002/anie.201108695.

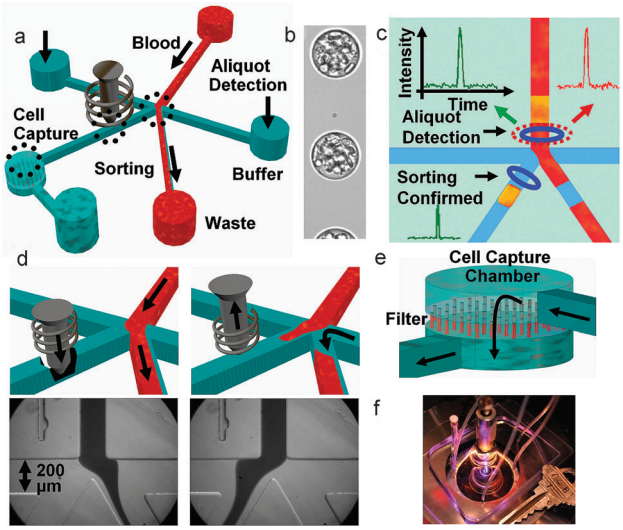

Figure 1. Schematic and images showing how eDAR works. a) Overview of the microfluidic chip. b) A high-speed camera image of whole blood aliquoted into a continuous stream of droplets surrounded by silicone oil. c) Aliquot detection: laser-induced fluorescence triggers the sorting of an aliquot containing a rare cell (shown in yellow) to the collection microchannel and cell capture chamber. d) Sorting: The solenoid piston is released to allow flow through the collection channel; images at the bottom show the flow of whole blood when the collection channel is closed (left) and opened (right). e) Cell capture: The collected aliquots are filtered through a membrane to remove blood cells from the target cells and leave the captured cells isolated and accessible for further study. f) Photograph of an eDAR chip.

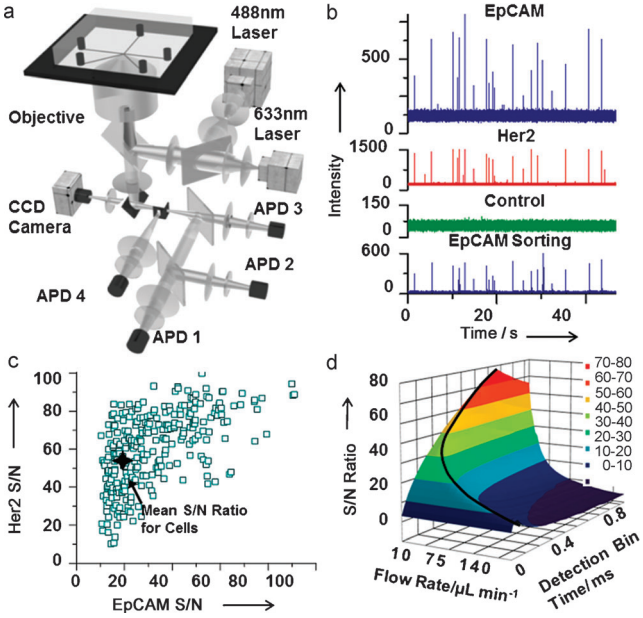

Figure 2. Aliquot detection system. a) The setup for aliquot detection is comprised of two excitation lasers and four APDs. b) A segment of the APD trace from clinical sample number 16 showing aliquots positive for the antibody markers EpCAM (top trace) and Her2 (second trace) that were correctly sorted (bottom trace). c) The S/N ratio for each single cell detected for both antibody labels from clinical sample number 16. d) S/N ratio for EpCAM-labeled single cells as a function of flow rate and signal bin time. The black curved line shows the optimal parameters with a maximum flow rate of 133 µL min^{-1} for a S/N ratio above 20.

robustness of the system. And finally, droplets were incompatible with the on-line filtration that we used to isolate the targeted CTCs from the other blood cells. Rather than creating physically isolated aliquots with droplets, therefore, we pursued the notion of virtual aliquots. Here, each aliquot was defined by a combination of the laser illumination volume, the bin time of the detection system, and the switching time of the solenoid. We found this approach offered the highest throughput and operational robustness. In our current system, 2 nL aliquots were the optimal compromise between detection sensitivity and throughput at a flow rate of 50 µL min^{-1}.

Once we defined an aliquot, we ranked the aliquot based on the presence or absence of rare cells (Figure 1). To detect rare cells in an aliquot, we labeled the cells with fluorescent antibodies against cell-surface markers characteristic of CTCs (see Table S1 in the Supporting Information). For breast cancer cells, for example, characteristic cell-surface markers are EpCAM and Her2 (all patients in this study were Her2 positive). Once labeling was complete, we introduced blood into the microfluidic chip at rates up to 80 µL min^{-1}. As an aliquot of blood passed through the detection region in the microfluidic channel, a laser illuminated it and excited any fluorescence labels that were present in the aliquot (Figure 1c). For each aliquot, the resulting fluorescence could be simultaneously collected at several (typically three) wavelengths using fiber-coupled avalanche photodiodes (APDs) to determine the contents of the aliquot. If the aliquot contained a target cell, the fluorescence emission triggered the sorting of that aliquot into the collection channel. Our system had two lasers at 488 and 633 nm for excitation (Figure 2), and fluorescence was collected through a rectangular confocal aperture and a series of dichroics and filters to fiber-coupled APDs:[25,26] APD1 detected the yellow fluorescence (560–590 nm) from the monoclonal antibody anti-EpCAM labeled with phycoerythrin (PE); APD2 was used as a negative control for the green wavelength range (500–550 nm) to eliminate false positives from broadly emitting fluorescent contaminants; and APD3 detected anti-Her2 labeled with Alexa-647 in the red wavelength band (640–690 nm). A second excitation region using only the 488 nm laser was located immediately after the sorting junction (Figure 1c); yellow fluorescence (560–590 nm) was collected in this spatially distinct detection region through a separate confocal aperture by APD4. This separate detection region confirmed, in real time, the accurate sorting of the blood aliquot with the target cell. The CTCs were readily detected in the 2 nL aliquots of blood with an average signal-to-noise (S/N) ratio of 32 for the EpCAM marker and 64 for the Her2 marker (Figure 2c). The S/N ratio was highly dependent on the flow rate of the cells as they went through the detection region as well as the detection bin time (Figure 2d). With our current system, the maximum flow rate that still allowed for an average S/N above 20 was 133 µL min^{-1}.

For this study, we simply ranked the aliquots as zero (no CTCs) or one (containing CTCs) but we envision more sophisticated rankings will be beneficial in the future, for

instance for aliquots with different types of rare cells. In comparison to the antibody-based surface capture of rare cells,[14] aliquot ranking offers more flexible logical operations. For example, we can collect aliquots based on the presence of EpCAM and Her2 and absence of fluorescence in the green channel; in antibody-based surface capture, cells that express either EpCAM or Her2 will be retained. Surface capture can only employ the "OR" logical operation while eDAR can make more complex logic decisions (see Figure S1 in the Supporting Information).

To test the sorting efficiency, we spiked cultured breast cancer cells (SKBr-3) into whole blood and labeled them with fluorescent anti-EpCAM antibodies. The blood was introduced into the microfluidic chip with flow rates varying between 10 and 80 μL min^{-1}. The sorting efficiency was defined as the number of aliquots triggered to be sorted compared to the number of cells detected as they entered the collection channel (Figure 3b and Figures S2 and S3 in the

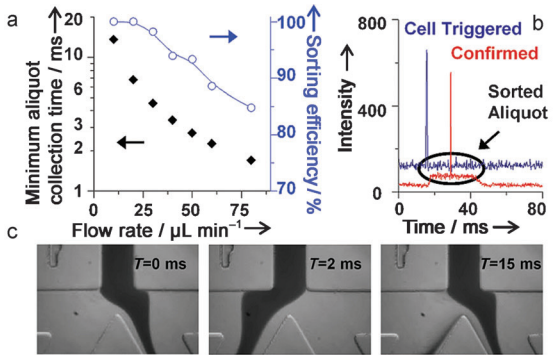

Figure 3. Aliquot sorting efficiency. a) A plot showing the minimum amount of time required to collect a desired aliquot of blood as a function of flow rate. The collection time was ca. 2.7 ms for 50 μL min^{-1}. The plot of sorting efficiency versus flow rate shows highly accurate sorting (up to 100%). b) Fluorescence trace from a CTC showing the triggering (blue) and successful sorting (red) of an aliquot of blood. c) High-speed camera images of the sorting junction before and after the release of the solenoid piston that show complete flow switching within 2 ms.

Supporting Information). At slow flow rates (25 μL min^{-1} and below), we got 100% sorting efficiency as the entire volume of each aliquot was collected (Figure 3a). At the fastest flow rate of 80 μL min^{-1}, only a portion of each aliquot was captured, resulting in a reduced sorting efficiency of 85%. The loss was caused by the collection channel not being completely open before the aliquot arrived because the solenoids do not have reproducible timing below 2 ms. There are several design improvements that could be made to increase the throughput, including increasing the distance between the detection region and the sorting junction, using a solenoid with sub-millisecond response times, and changing the channel dimensions.

Sorted aliquots flowed to the cell capture chamber where the target cells were retained by a filter. The majority of blood cells, including all RBCs and many small WBCs, passed through the filter (Figure 1e), which was a track-etched polycarbonate membrane with 5 μm pores that spanned the 1 mm diameter chamber (see Figure S4 in the Supporting Information). With such a small volume of blood (e.g. about 10 nL for 5 CTCs) coming into the collection chamber, the capacity of the around 1000 pores was more than adequate. Captured cells, which clogged the pores once trapped, did not significantly increase the pressure of the system, unlike bulk blood filtration systems where capacity issues are a primary concern.[27] The small size of the filtration chamber allowed for complete full-field imaging. The chamber was open and easily accessible from the top. Additional reagents, such as antibodies against various cellular targets, could be pipetted onto the filter and perfused over the targeted cells. Micropipettes could also be positioned above the filter to remove individual CTCs for analysis or culture.

Our process was optimized to include a minimum of sample preparation steps that did not involve lysing of RBCs. The blood processing consisted of labeling with antibodies, dilution with buffer, followed by centrifugation and removal of the supernatant containing the free antibodies (Figure S5 in the Supporting Information). Recovery experiments were conducted with two breast cancer cell lines, MCF-7 and SKBr-3. For our studies, the number of cells we spiked into blood was counted individually using a capillary cell-spiking method that we previously published.[28] This method allowed us to investigate the recovery rates conveniently for as few as five cells rather than the tens to thousands range that is typically reported.

The isolated cells were enumerated in the filtration area using laser-excited epifluorescence imaging of anti-EpCAM (Figure 4b) and anti-Her2 (Figure 4c). From nine separate recovery experiments using a flow rate of 50 μL min^{-1}, we determined the average recovery efficiency of the whole system was better than 93% (Figure 4a). The purity after the sorting step is variable, depending on the amount of WBCs presented in the blood sample, but is in the range of few tens of percent (10–50%). The purity after the entire process of imaging and selection is essentially 100%. This 50 μL min^{-1}

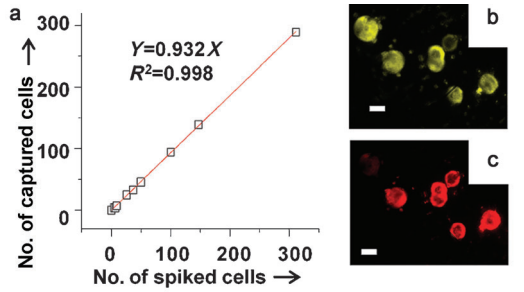

d Control run No.	1	2	3	4	5	6	7	8
No. of captured cells	0	0	0	0	0	0	0	0

Figure 4. Recovery efficiency for cultured cancer cells spiked into the whole blood from healthy donors. a) The average recovery efficiency for the nine runs is higher than 93% (Y is the number of captured cells, X is the number of spiked cells, and R^2 is the correlation coefficient). Fluorescence images of the captured cells on the filtration membrane labeled with b) anti-EpCAM and c) anti-Her2. The scale bar is 20 μm. d) Negative controls showing 8 control runs using healthy donor blood with zero false positives.

flow rate was used for the false positive experiments as well as for all the clinical samples.

Equally important is the potential for false positives. We performed negative control experiments using healthy donor blood. One milliliter of blood was labeled with anti-EpCAM and anti-Her2 antibodies and run through our system using the same protocol as used for the cell-recovery experiments and for processing clinical samples from breast cancer patients. Figure 4d shows the results from eight experiments, all of which found no target cells, yielding a false positive rate of zero.

To better understand the performance of eDAR, we carried out a side-by-side comparison between eDAR and the FDA-approved CellSearch assay using clinical samples. Patients with stage IV metastatic breast cancer had peripheral blood drawn in an outpatient cancer clinic as a part of their office visit. Multiple tubes of venipunctured blood were collected in each draw. The first tube was not used for cell analysis because of the potential for contamination from epithelial cells during the venipuncture process. Of the remaining tubes, one was drawn into a Veridex CellSave tube for enumeration using the Veridex CellSearch system. A second sample from the same draw was collected in a Vacutainer tube containing K3EDTA and delivered to our laboratory for analysis with eDAR. The samples were run independently: CellSearch was performed by a clinical technologist as part of routine clinical testing, and eDAR was carried out by our lab. The results of the CellSearch analysis were unknown to us until after we had completed the analysis of our samples. This arrangement allowed for a direct head-to-head comparison between the two systems.

For each clinical sample, we processed between 1 and 2 mL of the whole blood with a total sample preparation time of 40 min (Figure S5 and Table S2 in the Supporting Information). Each sample was run using a new disposable polydimethylsiloxan (PDMS) chip to prevent contamination. Aliquot sorting was triggered by the presence of anti-EpCAM-PE fluorescence. EpCAM was chosen because it is the primary marker used in the CellSearch system. For a 1 mL sample with a flow rate of 50 $\mu L\,min^{-1}$, each run took 20 min. The captured cells at the end of the run were imaged and analyzed using multi-color epifluorescence.

To confirm the presence of anti-EpCAM-PE, images were collected in the yellow wavelength region, 560 to 590 nm, by excitation with a 488 nm laser. To test for the presence of anti-Her2-Alexa 647, images were also collected in the red wavelength region at 650 to 690 nm, using a 633 nm laser. To count the number of CTCs, additional labeling with anti-CD45 and anti-cytokeratin was performed by directly pipetting the reagents onto the cells and washing the cells retained on the filter through the open top of the cell-capture chamber. For this secondary labeling step, the cells were first fixed with paraformaldehyde and permeabilized with a surfactant to allow binding of antibody to cytokeratin. The presence of CTCs was confirmed if they were labeled by anti-EpCAM and anti-cytokeratin but not anti-CD45, which is present on leukocytes. After this secondary labeling, the cells were further labeled with the nuclear stain DRAQ5 to confirm that the cells were intact. Figure 5a shows three cells from clinical sample number 16 that were positively labeled with EpCAM, Her2, cytokeratin, and DRAQ5 but were negative with the CD45 antibody.

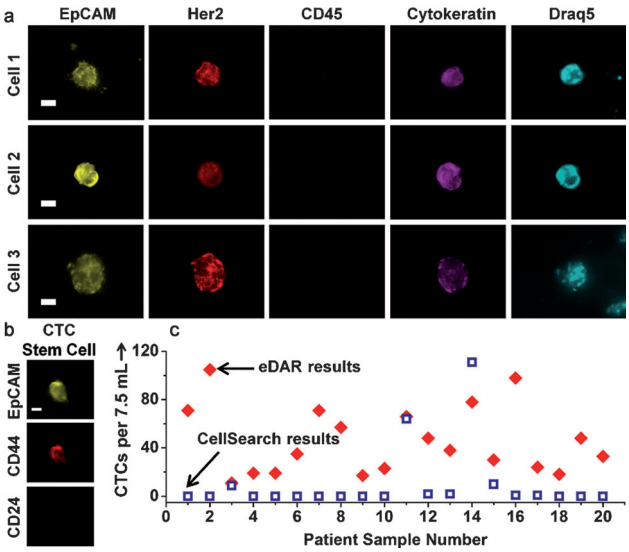

Figure 5. Clinical results for CTCs isolated from blood samples drawn from breast cancer patients. a) Images of three CTCs isolated from clinical sample number 16; the scale bar is 20 μm. b) Images from a CTC labeled with fluorescent antibodies against the breast cancer stem cell marker ($CD44^+/CD24^-$). c) Side-by-side comparison of clinical results from 20 breast cancer patient samples ran with CellSearch and eDAR.

Figure 5c summarizes the results from 20 clinical samples analyzed both by eDAR and CellSearch. The number of CTCs found by eDAR ranged from 11 to 105 for a normalized volume of 7.5 mL, with an average of 45. The CellSearch results from the same patient samples ranged from 0 to 111, with an average of 10. CellSearch found zero cells in 12 of the patient samples, with only four samples containing more than two CTCs. The eDAR process, in comparison, identified CTCs in all samples. The average of 10 CTCs enumerated by CellSearch is skewed by clinical sample 14. If we omit this sample from the analysis, CellSearch detected 0 to 64 CTCs with an average of five, while eDAR recovered 11 to 105 CTCs with an average of 44 (Table S2 in the Supporting Information). This comparison clearly illustrates the improved sensitivity offered by eDAR.

The eDAR process affords us the versatility of having the captured cells isolated in a small open area and retained by the filter where multiple analyses can be performed. Captured and labeled CTCs from clinical sample number 23 were first photobleached and then labeled with the stem cell markers anti-CD24-FITC and anti-CD44-Alexa-647 (Figure 5b). A study has shown that in breast cancer, the cell subpopulation that expresses the cell surface markers CD44 + and CD24-/low exhibits stem-cell characteristics.[5,29] Using eDAR, we were able to detect the presence of this subset of cells within the isolated CTCs from breast cancer patients.

In conclusion, the eDAR process represents a different approach than other techniques shown thus far for enumerating rare cells like CTCs. We believe it has the unique capability of recovering individual live CTCs with high

efficiency, throughput, and minimal stress. The eDAR feature of concentrating the isolated rare cells within a small easily assessable area bypasses the long imaging times that plague most other existing techniques and greatly increases its throughput. We believe eDAR will also find use in the isolation of other rare cells besides CTCs.

Received: December 10, 2011
Published online: February 22, 2012

Keywords: cancer · cell capture · cells · high-throughput screening · single-cell analysis

[1] M. Cristofanilli, G. Budd, M. Ellis, A. Stopeck, J. Matera, M. Miller, J. Reuben, G. Doyle, W. Allard, L. Terstappen, *N. Engl. J. Med.* **2004**, *351*, 781 – 791.
[2] W. Allard, J. Matera, M. Miller, M. Repollet, M. Connelly, C. Rao, A. Tibbe, J. Uhr, L. Terstappen, *Clin. Cancer Res.* **2004**, *10*, 6897 – 6904.
[3] C. B. M. Oudejans, M. L. Tjoa, B. A. Westerman, M. A. M. Mulders, I. J. Van Wijk, J. M. G. Van Vugt, *Prenatal Diagn.* **2003**, *23*, 111 – 116.
[4] M. Al-Hajj, M. S. Wicha, A. Benito-Hernandez, S. J. Morrison, M. F. Clarke, *Proc. Natl. Acad. Sci. USA* **2003**, *100*, 3983 – 3988.
[5] T. Reya, S. J. Morrison, M. F. Clarke, I. L. Weissman, *Nature* **2001**, *414*, 105 – 111.
[6] P. S. Steeg, *Nat. Med.* **2006**, *12*, 895 – 904.
[7] J. S. de Bono, A. Ashworth, *Nature* **2010**, *467*, 543 – 549.
[8] M. Alunni-Fabbroni, M. T. Sandri, *Methods* **2010**, *50*, 289 – 297.
[9] V. Zieglschmid, C. Hollmann, O. Bocher, *Crit. Rev. Clin. Lab. Sci.* **2005**, *42*, 155 – 196.
[10] S. Riethdorf, V. Mueller, L. Zhang, T. Rau, S. Loibl, M. Komor, M. Roller, J. Huober, T. Fehm, I. Schrader, J. Hilfrich, F. Holms, H. Tesch, H. Eidtmann, M. Untch, G. von Minckwitz, K. Pantel, *Clin. Cancer Res.* **2010**, *16*, 2634 – 2645.
[11] G. Vona, A. Sabile, M. Louha, V. Sitruk, S. Romana, K. Schutze, F. Capron, D. Franco, M. Pazzagli, M. Vekemans, B. Lacour, C. Brechot, P. Paterlini-Brechot, *Am. J. Pathol.* **2000**, *156*, 57 – 63.
[12] T. Xu, B. Lu, Y. Tai, A. Goldkorn, *Cancer Res.* **2010**, *70*, 6420 – 6428.
[13] J. S. Kuo, Y. X. Zhao, P. G. Schiro, L. Y. Ng, D. S. W. Lim, J. P. Shelby, D. T. Chiu, *Lab Chip* **2010**, *10*, 837 – 842.
[14] S. Nagrath, L. V. Sequist, S. Maheswaran, D. W. Bell, D. Irimia, L. Ulkus, M. R. Smith, E. L. Kwak, S. Digumarthy, A. Muzikansky, P. Ryan, U. J. Balis, R. G. Tompkins, D. A. Haber, M. Toner, *Nature* **2007**, *450*, 1235 – 1239.
[15] U. Dharmasiri, S. K. Njoroge, M. A. Witek, M. G. Adebiyi, J. W. Kamande, M. L. Hupert, F. Barany, S. A. Soper, *Anal. Chem.* **2011**, *83*, 2301 – 2309.
[16] S. T. Wang, K. Liu, J. A. Liu, Z. T. F. Yu, X. W. Xu, L. B. Zhao, T. Lee, E. K. Lee, J. Reiss, Y. K. Lee, L. W. K. Chung, J. T. Huang, M. Rettig, D. Seligson, K. N. Duraiswamy, C. K. F. Shen, H. R. Tseng, *Angew. Chem.* **2011**, *123*, 3140 – 3144; *Angew. Chem. Int. Ed.* **2011**, *50*, 3084 – 3088.
[17] R. T. Krivacic, A. Ladanyi, D. N. Curry, H. B. Hsieh, P. Kuhn, D. E. Bergsrud, J. F. Kepros, T. Barbera, M. Y. Ho, L. B. Chen, R. A. Lerner, R. H. Bruce, *Proc. Natl. Acad. Sci. USA* **2004**, *101*, 10501 – 10504.
[18] J. D. Adams, P. Thevoz, H. Bruus, H. T. Soh, *Appl. Phys. Lett.* **2009**, *95*, 254103.
[19] P. Balasubramanian, L. Y. Yang, J. C. Lang, K. R. Jatana, D. Schuller, A. Agrawal, M. Zborowski, J. J. Chalmers, *Mol. Pharm.* **2009**, *6*, 1402 – 1408.
[20] H. B. Hsieh, D. Marrinucci, K. Bethel, D. N. Curry, M. Humphrey, R. T. Krivacic, J. Kroener, L. Kroener, A. Ladanyi, N. Lazarus, P. Kuhn, R. H. Bruce, J. Nieva, *Biosens. Bioelectron.* **2006**, *21*, 1893 – 1899.
[21] H. J. Gross, B. Verwer, D. Houck, R. A. Hoffman, D. Recktenwald, *Proc. Natl. Acad. Sci. USA* **1995**, *92*, 537 – 541.
[22] M. Y. He, J. S. Edgar, G. D. M. Jeffries, R. M. Lorenz, J. P. Shelby, D. T. Chiu, *Anal. Chem.* **2005**, *77*, 1539 – 1544.
[23] J. S. Edgar, G. Milne, Y. Q. Zhao, C. P. Pabbati, D. S. W. Lim, D. T. Chiu, *Angew. Chem.* **2009**, *121*, 2757 – 2760; *Angew. Chem. Int. Ed.* **2009**, *48*, 2719 – 2722.
[24] T. Schneider, D. Burnham, G. Yen, L. Huynh, D. T. Chiu, unpublished results.
[25] P. G. Schiro, C. L. Kuyper, D. T. Chiu, *Electrophoresis* **2007**, *28*, 2430 – 2438.
[26] G. D. M. Jeffries, R. M. Lorenz, D. T. Chiu, *Anal. Chem.* **2010**, *82*, 9948 – 9954.
[27] S. Zheng, H. Lin, J. Q. Liu, M. Balic, R. Datar, R. J. Cote, Y. C. Tai, *J. Chromatogr. A* **2007**, *1162*, 154 – 161.
[28] Y. Zhao, P. G. Schiro, J. Kuo, L. Ng, D. T. Chiu, *Anal. Chem.* **2009**, *81*, 1285 – 1290.
[29] D. Ponti, A. Costa, N. Zaffaroni, G. Pratesi, G. Petrangolini, D. Coradini, S. Pilotti, M. A. Pierotti, M. G. Daidone, *Cancer Res.* **2005**, *65*, 5506 – 5511.

